

ORIGINAL ARTICLE

Transcription factor ETV4 promotes the development of hepatocellular carcinoma by driving hepatic TNF- α signaling

Dandan Qi¹ | Min Lu^{1,2} | Pengfei Xu³ | Xinli Yao^{1,2} | Yongchen Chen^{1,2} |
 Lipeng Gan^{1,2} | Yong Li^{1,2} | Yahua Cui⁴ | Xiaomei Tong¹ | Shuhong Liu³ |
 Jingmin Zhao³ | Ningning Liu¹ | Xin Ye^{1,2} 

¹Key Laboratory of Pathogenic Microbiology and Immunology, Institute of Microbiology, Chinese Academy of Sciences, Beijing, P. R. China

²Savaid Medical School, University of Chinese Academy of Sciences, Beijing, P. R. China

³The Fifth Medical Center of Chinese People's Liberation Army General Hospital, Beijing, P. R. China

⁴School of Life Sciences, University of Science and Technology of China, Hefei, Anhui, P. R. China

Correspondence

Xin Ye, Key Laboratory of Pathogenic Microbiology and Immunology, Institute of Microbiology, Chinese Academy of Sciences (CAS), Beijing 100101, China.
 Email: yex@im.ac.cn

Ningning Liu, Key Laboratory of Pathogenic Microbiology and Immunology, Institute of Microbiology, Chinese Academy of Sciences, Beijing 100101, China.

Email: liunn@im.ac.cn

Abstract

Background: Hepatic inflammation is the major risk factor of hepatocellular carcinoma (HCC). However, the underlying mechanism by which hepatic inflammation progresses to HCC is poorly understood. This study was designed to investigate the role of ETS translocation variant 4 (ETV4) in linking hepatic inflammation to HCC.

Methods: Quantitative real-time PCR and immunoblotting were used to detect the expression of ETV4 in HCC tissues and cell lines. RNA sequencing and luciferase reporter assays were performed to identify the target genes of ETV4. Hepatocyte-specific *ETV4*-knockout (*ETV4*^{fl/fl, alb-cre}) and transgenic (*ETV4*^{Hep-TG}) mice and diethylnitrosamine-carbon tetrachloride (DEN-CCL₄)

List of Abbreviation: ETV4, ETS translocation variant 4; HCC, hepatocellular carcinoma; NASH, nonalcoholic steatohepatitis; HBV, Hepatitis B virus; Alb-Cre, Cre driven by albumin promoter; TNF- α , tumor necrosis factor alpha; IL-6, interleukin-6; MAPK11, mitogen-activated protein kinase 11; CCL₄, carbon tetrachloride; TERT, telomerase reverse transcriptase; IKK- β , nuclear factor kappa-B kinase subunit beta; NF- κ B, nuclear factor kappa B; STAT3, signal transducer and activator of transcription 3; TNFR1, TNF receptor 1; MYC, myelocytomatosis oncogene; DEN, diethylnitrosamine; MMP, matrix metalloproteinase; shRNAs, short hairpin RNAs; CDKN1A, cyclin-dependent kinase inhibitor 1; HFD, high fat diet; CDE, choline-deficient and ethionine-supplemented diet; CH, cholestasis induced hepatitis; YAP, Yes-associated protein; TEAD, TEA domain family member; uPA, urokinase plasminogen activator; CXCL1, C-X-C motif chemokine ligand 1; CXCL5, C-X-C motif chemokine ligand 5; PD-L1, programmed cell death 1 ligand 1; CCL2, C-C motif chemokine ligand 2; ROS, reactive oxygen species; ATCC, American type culture collection; GEPIA, gene expression profiling interactive analysis; LIHC, liver hepatocellular carcinoma; NCBI GEO, national center for biotechnology information gene expression omnibus; IHC, Immunohistochemistry; KEGG, Kyoto encyclopedia of genes and genomes; CHIP, chromatin immunoprecipitation; H&E, hematoxylin and eosin; BSA, bovine serum albumin; ELISA, enzyme-linked immunosorbent assay; ANOVA, analysis of variance..

Dandan Qi and Min Lu contributed equally to this work.

This is an open access article under the terms of the [Creative Commons Attribution-NonCommercial-NoDerivs](https://creativecommons.org/licenses/by-nc-nd/4.0/) License, which permits use and distribution in any medium, provided the original work is properly cited, the use is non-commercial and no modifications or adaptations are made.

© 2023 The Authors. *Cancer Communications* published by John Wiley & Sons Australia, Ltd. on behalf of Sun Yat-sen University Cancer Center.

Jingmin Zhao, The Fifth Medical Center of Chinese PLA General Hospital, Beijing 100039, China.
Email: jmzhao302@163.com

Funding information

National Key R&D Program of China, Grant/Award Numbers: 2022YFC2303400, 2022YFC2305205; Strategic Priority Research Program of the Chinese Academy of Sciences, Grant/Award Number: XDB29010000

treatment experiments were applied to investigate the function of ETV4 *in vivo*. The Cancer Genome Atlas (TCGA) database mining and pathological analysis were carried out to determine the correlation of ETV4 with tumor necrosis factor- α (TNF- α) and mitogen-activated protein kinase 11 (MAPK11).

Results: We revealed that ETV4 was highly expressed in HCC. High levels of ETV4 predicted a poor survival rate of HCC patients. Then we identified ETV4 as a transcription activator of TNF- α and MAPK11. ETV4 was positively correlated with TNF- α and MAPK11 in HCC patients. As expected, an increase in hepatic TNF- α secretion and macrophage accumulation were observed in the livers of *ETV4^{Hep-TG}* mice. The protein levels of TNF- α , MAPK11, and CD68 were significantly higher in the livers of *ETV4^{Hep-TG}* mice compared with wild type mice but lower in *ETV4^{fl/fl, alb-cre}* mice compared with *ETV4^{fl/fl}* mice as treated with DEN-CCL₄, indicating that ETV4 functioned as a driver of TNF- α /MAPK11 expression and macrophage accumulation during hepatic inflammation. Hepatocyte-specific knockout of ETV4 significantly prevented development of DEN-CCL₄-induced HCC, while transgenic expression of ETV4 promoted growth of HCC.

Conclusions: ETV4 promoted hepatic inflammation and HCC by activating transcription of TNF- α and MAPK11. Both the ETV4/TNF- α and ETV4/MAPK11 axes represented two potential therapeutic targets for highly associated hepatic inflammation and HCC. ETV4+TNF- α were potential prognostic markers for HCC patients.

KEYWORDS

ETV4, TNF- α , MAPK11, macrophage, hepatocellular carcinoma, hepatic inflammation

1 | BACKGROUND

Liver cancer is the second most lethal cancer, with a very low 5-year survival rate. Each year, 905,000 new liver cancer cases are diagnosed, and 830,000 liver cancer-related deaths occur [1]. Liver cancer accounts for 4.7% of all new cancer cases and 8.3% of all cancer-related deaths [1]. Hepatocellular carcinoma (HCC) accounts for 80% of liver cancer cases and is the most common form of liver cancer [2, 3]. Hepatitis B virus (HBV) and hepatitis C virus infection, alcohol abuse, obesity and diabetes-associated nonalcoholic steatohepatitis (NASH) are the main risk factors for HCC [4, 5]. Although the incidence of alcoholic hepatitis and metabolic syndrome-related NASH is increasing faster in western countries, HBV infection remains the major risk factor for HCC in China [6, 7].

Sustained inflammation accelerated the development and aggressiveness of HCC by promoting the survival of hepatocytes [8, 9], enhancing angiogenesis [10], increasing HCC escape of immune surveillance [11], and enhancing invasion and metastasis [12, 13]. Interleukin-6 (IL-6)

produced by Kupffer cells activated the signal transducer and activator of transcription 3 (STAT3) pathway in hepatocytes and induced the transcription of myelocytomatosis oncogene (MYC), B-cell lymphoma-2 (BCL-2) and Cyclin B to promote the proliferation and survival of hepatocytes [14, 15]. Tumor necrosis factor- α (TNF- α) activated the downstream inhibitor of nuclear factor kappa-B kinase subunit beta (IKK- β)/nuclear factor kappa B (NF- κ B) signaling pathway and increased the number and size of diethylnitrosamine (DEN)-induced mouse HCC tumors [16]. Lymphotoxin α/β expression induced chronic liver injury and hepatitis, which further stimulated the compensatory proliferation of hepatocytes and led to tumorigenesis [17]. Both dietary and genetic obesity enhanced liver inflammation and carcinogenesis by inducing TNF- α and IL-6 expression [14, 15]. TNF receptor 1 (TNFR1)-deficient mice had decreased tumor formation than wild-type mice when DEN and a high-fat diet (HFD) were used to induce HCC tumorigenesis [18]. Inflammation played a key role in HCC development, and inflammatory cytokines were reported mainly expressed in

immune cells. It has been reported that inflammatory cell-secreted TNF- α played a critical role in inducing chronic inflammation of the liver [19–21], and macrophage infiltration had important impact on tumor progression [22]. However, the mechanisms of hepatocytes secreting TNF- α during HCC development and efficacy of TNF- α on regulating macrophages infiltration were unclear.

ETV4 is a transcription factor which belongs to the E26 transformation-specific (ETS) family. All the members of this family have a conserved ETS DNA-binding motif. It has been reported that ETV4 played an important role in tissue development, such as neuronal differentiation and kidney morphogenesis [23]. ETV4 was also defined as an oncogene that promoted the growth and metastasis of gastric cancer and the development of prostate cancer [24]. However, the detailed mechanism of how ETV4 regulating inflammation is not fully elucidated.

In this study, we focused on the function of ETV4 in liver inflammation and HCC development. We investigated the association of ETV4 with HCC formation by analyzing the clinical samples and diethylnitrosamine (DEN)-carbon tetrachloride (CCL₄)-induced HCC mice. We explored the functions of ETV4 in liver inflammation via acute and chronic liver inflammation mouse model. These studies were expected to uncover the mechanisms of ETV4 regulating liver inflammation and HCC formation.

2 | MATERIALS AND METHODS

2.1 | Cell lines

The human embryonic kidney cell line 293T were purchased from American Type Culture Collection (ATCC) (Manassas, VA, USA). The human hepatoma cell line HepG2 were purchased National Collection of Authenticated Cell Cultures (Shanghai, China). The HBV transgenic cell line HepG2-4D14 and human hepatoma cell line Huh7 were gifts from Dr. Dongping Xu (The Fifth Medical Center of Chinese PLA General Hospital, Beijing, China). The Huh7 cell was verified by short tandem repeat sequence in 2023. All the cell lines were cultured in Dulbecco's modified Eagle's medium (DMEM, 12800-017, Gibco, Carlsbad, CA, USA) supplemented with 10% fetal bovine serum (FBS, ST30-3302, PAN-Biotech, Aidenbach, Germany).

2.2 | Datasets and analysis

The differentially expressed genes (DEGs) in HCC tissues compared to normal tissues were downloaded from Gene Expression Profiling Interactive Analysis (GEPIA) in

which the RNA expression data from the Cancer Genome Atlas (TCGA, <http://gepia.cancer-pku.cn/>) were analyzed, and they were overlapped with the DEGs in HepG2-4D14 compared to HepG2 cells. The Cancer Genome Atlas Liver Hepatocellular Carcinoma (TCGA-LIHC) datasets were downloaded from TCGA, and the *ETV4* mRNA level in tumors and normal tissues was analyzed. GSE64041, GSE83148, GSE94660 and GSE84005 were obtained from National Center for Biotechnology Information Gene Expression Omnibus (NCBI GEO) profiles, and the relative *ETV4* mRNA level in these cohorts was analyzed. JASPAR (<https://jaspar.genereg.net/>) was used to predict the ETV4-binding sites on the promoter of *TNF- α* or *MAPK11*. HCC single-cell transcriptome data were from public database (<https://db.cngb.org/PRHCCdb/>), in which the expression profiles of tumor cells and different kinds of immune cells were obtained [25]. xCell (<https://comphealth.ucsf.edu/app/xcell>) was used to perform cell type enrichment analysis from gene expression data, and enumerate immune cell subsets from TCGA-LIHC transcriptomes [26].

2.3 | Patient samples

Twenty-seven HCC tumor tissues and paired peritumoral tissues were defined as Cohort 1 in which the patients were underwent surgery between August 2012 and December 2014. Total RNA was extracted from all the tumor tissues and nontumor tissues and analyzed by quantitative real-time PCR (qRT-PCR) to measure *ETV4* mRNA levels. A total of 128 formalin-fixed paraffin-embedded (FFPE) primary HCC liver specimens were defined as Cohort 2 and subjected to Immunohistochemistry (IHC) staining for ETV4, TNF- α , MAPK11 and CD68. Patients in Cohort 2 were hospitalized and underwent surgery between Jun 2012 and Dec 2013. The patients were all diagnosed with primary HCC, with no cholangiocarcinoma or other cancers. Patients in Cohort 2 were divided into HBV-low (≤ 40 DNA copies/mL) and HBV-high (> 40 DNA copies/mL) groups according to the serum HBV DNA copy number before surgery. Sixty-six HCC patients who underwent surgery between July 2012 and November 2013 were defined as Cohort 3. The patients in Cohort 3 were divided into HBV-negative (both HBsAg and HBeAg were negative, and HBV DNA was undetectable in serum) and HBV-positive groups. The clinical characteristics of the enrolled patients are listed in Supplementary Table S1. All the patient samples were collected from the Fifth Medical Center of Chinese PLA General Hospital. All the participants provided written informed consent. The patient samples were assigned arbitrary identification numbers based on the order of enrollment.

For the single-marker overall survival (OS) analyses, the quartile was used to set the group cutoff according to the levels of ETV4, TNF- α or MAPK11. The top 25% was classified as high, the bottom 25% was classified as low, and the medium 50% was classified as intermediate.

For the double-marker OS analyses, firstly the medium was used to set the group cutoff according to the levels of ETV4, TNF- α or MAPK11, in which the top 50% was classified as high, the other 50% was classified as low. Then, patients with both ETV4-high and TNF- α -high were defined as ETV4+TNF- α -high, while patients with both ETV4-low and TNF- α -low were defined as ETV4+TNF- α -low. The other patients were classified as intermediate. The same group classification was applied for ETV4+MAPK11 groups.

2.4 | Real-time quantitative PCR (qRT-PCR)

The human and mouse liver tissues were homogenized with the tissue grinder. Total RNA was extracted from tissues and cell lines with TRIzol (1559608, Invitrogen, Carlsbad, CA, USA). cDNA was synthesized with Hifair II 1st strand cDNA Synthesis SuperMix (11123ES60, YEASEN, Shanghai, China). The random and oligo(dT)s primer mixtures were used for the cDNA synthesis. The reaction mixture was pre-denatured for 5 min at 95°C, then denatured for 10 s at 95°C, annealed and extended for 30 s at 60°C, for a total 40 cycles. qRT-PCR was performed with qPCR SYBR Green Master Mix (11202ES08, YEASEN, Shanghai, China). The primers specific for the indicated genes used in qRT-PCR are listed in Supplementary Table S2.

2.5 | RNA sequencing and analysis

The human *ETV4* gene was cloned into the lentiviral vector pLL-IRES-puro (provided by Dr. Wenjun Liu, Institute of Microbiology, Chinese Academy of Sciences, Beijing, China) and named as pLL-*ETV4*. Short hairpin RNAs (shRNAs) targeting human *ETV4* were cloned into the pSIH1-GFP lentiviral plasmid. The pLL-*ETV4* vector or the pSIH1-GFP-sh*ETV4* vector and the lentivirus packing plasmids were co-transfected into 293T cells. Lentivirus was harvested 72 h post transfection. HepG2 cells were infected with lentivirus carrying *ETV4* to build the *ETV4*-overexpressing HepG2 cells (HepG2-*ETV4*-oe). Huh7 cells were infected with lentivirus carrying *ETV4* shRNA to build the *ETV4*-knockdown Huh7 cells (Huh7-sh*ETV4*). Total RNA was extracted from HepG2-*ETV4*-oe and control cells or Huh7-sh*ETV4* and control cells. The

mRNAs were enriched and subjected to mRNA library construction and sequencing by BGI (BGISEQ-500 platform, Shenzhen, China). The raw reads were filtered and quantity controlled to obtain clean reads. Then, the clean reads were aligned with the *Homo sapiens* genome (GCF_000001405.37_GRCh38.p11). The gene abundance was measured in fragments per kilobase of exon per million fragments mapped (FPKM). The genes with fold change higher or lower than 2 in HepG2-*ETV4*-oe vs HepG2 cells, or Huh7-sh*ETV4* vs. Huh7 cells, were defined as DEGs. The DEGs within the groups were further analyzed with Kyoto Encyclopedia of Genes and Genomes (KEGG) for signaling pathway enrichment.

2.6 | Dual-luciferase reporter assay

Human *TNF- α* and *MAPK11* promoters and their mutants were cloned into the pGL4 basic vector. HEK293T cells were seeded in 24-well plates (3×10^5 cells per well) and transfected with the pLL-*ETV4* or control vector together with the pGL4-*TNF- α* /*MAPK11* promoter and pRL-TK Renilla reporter plasmids as an internal control for 24 h. Then, the cell lysates were harvested and subjected to luciferase assay with the dual-specific luciferase reporter assay system (E1980, Promega, Madison, WI, USA).

2.7 | Chromatin immunoprecipitation (CHIP) assay

The CHIP assay was performed with the CHIP assay kit (P2078, Beyotime, Wuhan, Hubei, China). Briefly, Huh7 cells were cross-linked with 4% formaldehyde for 10 min, then treated with 125 mmol/L glycine for 5 min. Cells were collected and sonicated. The samples were centrifuged for 10 min at 8,000 g at 4°C. The supernatants were subjected to immunoprecipitation (IP) with IgG or anti-*ETV4* antibodies for 4 h, followed by incubation with protein A Sepharose beads for 2 h. The IP samples were eluted and treated with proteinase K, and then the DNA were extracted with phenol-chloroform and subjected to qRT-PCR with indicated primers.

2.8 | Mouse models

C57BL/6 *ETV4* conditional knockout mice (*ETV4*^{fl/fl}, alb-cre) were generated with the CRISPR/Cas9-guided homologous recombination system (Biocytogen, Beijing, China). Briefly, an *ETV4* targeting vector containing the *ETV4* genome sequence from exon 6 to exon 13 with 5'loxP and 3'loxP flanking sites was constructed. Small guide RNA

(sgRNA) sequences that effectively targeted intron 6 and the downstream sequence of exon 13 were selected with the UCATM assay, and Cas9/sgRNA plasmids were constructed. The *ETV4* targeting vector and Cas9/sgRNA plasmids were microinjected into zygotes from the oviducts of 4-week-old female C57BL/6 mice. The genotype of 7-day-old male and female *ETV4*^{fl/fl} mice was confirmed by Southern blotting and DNA sequencing. For Southern blotting, the genomic DNA was digested with AseI, and then subjected to hybridization with digoxin-labeled probe of *ETV4* exon 5. Hepatocyte-specific *ETV4*^{fl/fl, alb-cre} mice were generated by crossing *ETV4*^{fl/fl} mice with Alb-Cre mice.

To generate hepatocyte-specific *ETV4* conditional transgenic mice (*ETV4*^{Rosa26-floxp-gfp-floxp-mETV4/+}, alb-cre, *ETV4*^{Hep-TG}), floxp-gfp-polyA-floxp mouse *ETV4* (*mETV4*) was inserted into the Rosa26 locus of C57BL/6 wild type mice. Rosa26 is a non-coding gene on chromosome 6 of the mice. In general, the gene inserted into Rosa26 locus can be expressed normally while did not affect the expression of neighboring genes. The *ETV4*^{Hep-TG} mice were generated by crossing *ETV4*^{Rosa26-floxp-gfp-floxp-mETV4/+} mice with Alb-Cre mice.

HCC mouse model was generated as follows: 2-week-old male *ETV4*^{fl/fl} and *ETV4*^{fl/fl, alb-cre} or wild type and *ETV4*^{Hep-TG} mice were intraperitoneally injected with 25 mg/kg DEN (N0756, Sigma Aldrich, Saint Louis, MO, USA), followed by intraperitoneally injection of 0.5 mL/kg CCL₄ (C0731530924, Nanjing Reagent, Nanjing, China) every two weeks. The mice were euthanized via cervical dislocation at the 21-week-old. The livers were harvested and imaged, and the tumor number and size were measured. Hematoxylin and eosin (H&E) staining was performed and scanned by Leica digital pathology scanner Aperio CS2 (Wetzlar, Germany). The numbers of microscopic tumors were counted. The diameter of the tumor and the total tissue area were measured by Image Scope. Numbers of tumors per cm² were calculated.

For the acute inflammation model, 8-week-old male wild type and *ETV4*^{Hep-TG} mice were intraperitoneally injected with DEN (100 mg/kg) for 8 h and euthanized. Then the livers were fixed with formalin and subjected to IHC staining.

To establish chronic inflammation model, 2-week-old male *ETV4*^{fl/fl} and *ETV4*^{fl/fl, alb-cre} or wild type and *ETV4*^{Hep-TG} mice were intraperitoneally injected with a single dose of DEN (25 mg/kg), followed by CCL₄ (0.5 mL/kg) treatment every two weeks, and euthanized at 16 weeks. The livers were fixed with formalin and subjected to H&E staining or IHC staining with the indicated antibodies.

To deplete macrophages, 8-week-old male wild type and *ETV4*^{Hep-TG} mice were intravenously injected with 10

mg/kg GdCl₃ (203289, Sigma Aldrich, Saint Louis, MO, USA) every two days for 3 times [27, 28].

All the mice in this study were housed under specific pathogen-free (SPF) conditions at 25°C with 50% humidity. The mice were euthanized via cervical dislocation at the end of experiments. All the experiments were approved by the Ethical Review Committee of the Institute of Microbiology, Chinese Academy of Sciences (APIMCAS2019009).

2.9 | IHC analysis

The human and mouse FFPE samples were sliced in 5 mm thickness and subjected to standard IHC procedures. In brief, the sections were treated with xylene firstly, and then hydrated in series of ethanol (99.9% ethanol, 95% ethanol, 75% ethanol, 50% ethanol, H₂O). The antigen retrieval was performed as follows: for *ETV4* and TNF- α , the sections were treated with 1 mmol/L EDTA/10 mmol/L Tris HCl (pH 9.0); for MAPK11 and CD68, the sections were treated with 10 mmol/L sodium citrate (pH 6.0) for 30 min. The sections were blocked with 5% bovine serum albumin (BSA) (0032, Amresco, Solon, OH, USA) and incubated with primary antibodies (anti-*ETV4*, 1:50, overnight at 4°C; anti-MAPK11, 1:125, 2.5 h at room temperature; anti-TNF- α , 1:500, 2.5 h at room temperature; anti-CD68, 1:300, overnight at 4°C) and then incubated with horseradish peroxidase (HRP)-conjugated secondary antibody (PV-9000, ZSGB-BIO, Beijing, China) for 40 min at room temperature. The whole slide image was scanned by a NanoZoomer 2.0 HT (Hamamatsu, Japan) and analyzed with a HALO 2.3 digital pathology analysis system (Indica Labs, NM, USA). The tumor and adjacent non-tumor areas were manually defined by using the HALO software (Albuquerque, NM, USA). The average density and percentage of positive cells for H-score was calculated with the equation: H-score = weak positive cell percentage \times 1 + moderately positive cell percentage \times 2 + strongly positive cell percentage \times 3.

2.10 | Primary mouse hepatocyte isolation

Mouse primary hepatocytes were isolated according to the procedures of Wen Zhang's Lab (<http://www.mouselivercells.com/>). Briefly, 8-week-old wild type or *ETV4*^{Hep-TG} male mice were anesthetized by intraperitoneally injection of 400 μ g/g 2,2,2-tribromoethanol (T48402, Sigma Aldrich, Saint Louis, MO, USA), and then perfused with 100 units/mL type IV collagenase (17104, Gibco, Carlsbad, CA, USA) via

the portal vein for 3-5 min until the livers were digested sufficiently. The livers were dissected out and teared apart to release the hepatocytes. The hepatocytes were collected after centrifugation (3 min, 50 g at 4°C) and plated. The *ETV4*, *TNF- α* and *MAPK11* mRNA levels were measured by qRT-PCR.

2.11 | Enzyme-linked immunosorbent assay (ELISA)

HepG2 cells overexpressing *ETV4* or control cells were seeded in 24-well plates (2×10^5 cells per well) for 36 h. Then, the supernatants were collected and subjected to ELISA with a human TNF- α ELISA kit (KIT10602, Sino Biological, Beijing, China).

2.12 | Flow cytometry analysis

The mouse livers were minced into 1 mm³ pieces, followed by digestion with collagenase for 30 min. The cells were centrifuged at 350 g at 4°C for 3 min, and purified in 40% percoll. Subsequently, the cells were stained with anti-CD68 (137009, FA-11), anti-F4/80 (123110, BM8), anti-CD45 (103115, 30-F11), anti-CD11b (101212, M1/70), anti-CD3 (100205, 17A2), anti-CD4 (100515, RM4-5), anti-CD8 (100733, 53-6.7), anti-Ly6G (127617, 1A8) antibodies (BioLegend, San Diego, CA, USA), and sorted using a BD FACSAria II Cell Sorter (BD Bioscience, San Jose, CA, USA).

2.13 | Statistical analysis

The OS of HCC patients after diagnosis was analyzed with the Kaplan-Meier estimator and calculated with the log-rank test. Student *t* test was used for two-group comparisons, and two-way analysis of variance (ANOVA) was used for multiple-group comparisons. $P < 0.05$ was considered significance.

3 | RESULTS

3.1 | The level of *ETV4* was negatively associated with the survival of HCC patients

To investigate the HBV-related genes involved in the development of HCC, we overlapped the DEGs in the HBV transgenic cell line HepG2-4D14 compared to the parental cell line HepG2 and the DEGs in HCC tumor tissues

compared to normal tissues in the TCGA-LIHC cohort (Figure 1A). Sixty-nine overlapped genes were identified (Supplementary Table S3), and the differential expression pattern is shown in Figure 1B. Among these 69 genes, *ETV4* expression level was the most significantly associated with the OS of HCC patients (Supplementary Figure S1A), and the mRNA level of *ETV4* was much higher in tumor tissues than in normal tissues according to the data from TCGA (Supplementary Figure S1B) and GEO HCC datasets (Supplementary Figure S1C). We next compared the mRNA level of *ETV4* in 27 pairs of HCC tissues and their paired adjacent peritumoral tissues, and found that *ETV4* was upregulated in HCC tumor tissues comparing to their paired adjacent peritumoral tissues (Figure 1C). The HCC datasets from GEO also showed that *ETV4* was higher in tumors than in their paired peritumoral tissues (Supplementary Figure S1C-E). Then, we performed IHC staining of *ETV4* in 128 HCC liver tissues which were collected from patients who underwent surgery between 2012 and 2013. The mean intensity of *ETV4* staining was evaluated and representative images are shown in Figure 1D. Kaplan-Meier analysis demonstrated that patients with higher *ETV4* levels had poorer survival rate (Figure 1E), which was consistent with the results shown in Supplementary Figure S1A, and both the percentage of *ETV4*-positive cells (Figure 1F) and the H-score (Supplementary Figure S1F) were higher in tumor tissues than in paired adjacent peritumoral tissues. All these data demonstrated that *ETV4* was highly expressed in HCC tumor tissue, indicating that *ETV4* level might predict poor survival rate of HCC patients.

3.2 | *ETV4* expression was upregulated in HBV-positive HCC and chronic hepatitis liver tissues

Both *ETV4* mRNA and protein levels were higher in HepG2-4D14 cells than in parental HepG2 cells (Supplementary Figure S1G-H), which is consistent with the results in Figure 1B. We analyzed the relative *ETV4* level in the GEO dataset (GSE83148), which included gene expression data from 122 liver samples from chronic hepatitis B (CHB) patients and 6 liver samples from healthy controls. The results indicated that the mRNA level of *ETV4* was higher in the CHB samples than in the normal samples (Supplementary Figure S1I). Also, the mRNA levels of *ETV4* were higher in tumor tissues from HBV-positive patients than in those from HBV-negative patients in Cohort 3 (Figure 1G). We then divided the HCC samples in Cohort 2 into two groups (HBV-low and HBV-high) according to the HBV DNA copy numbers in the serum of patients before surgery. The data of IHC

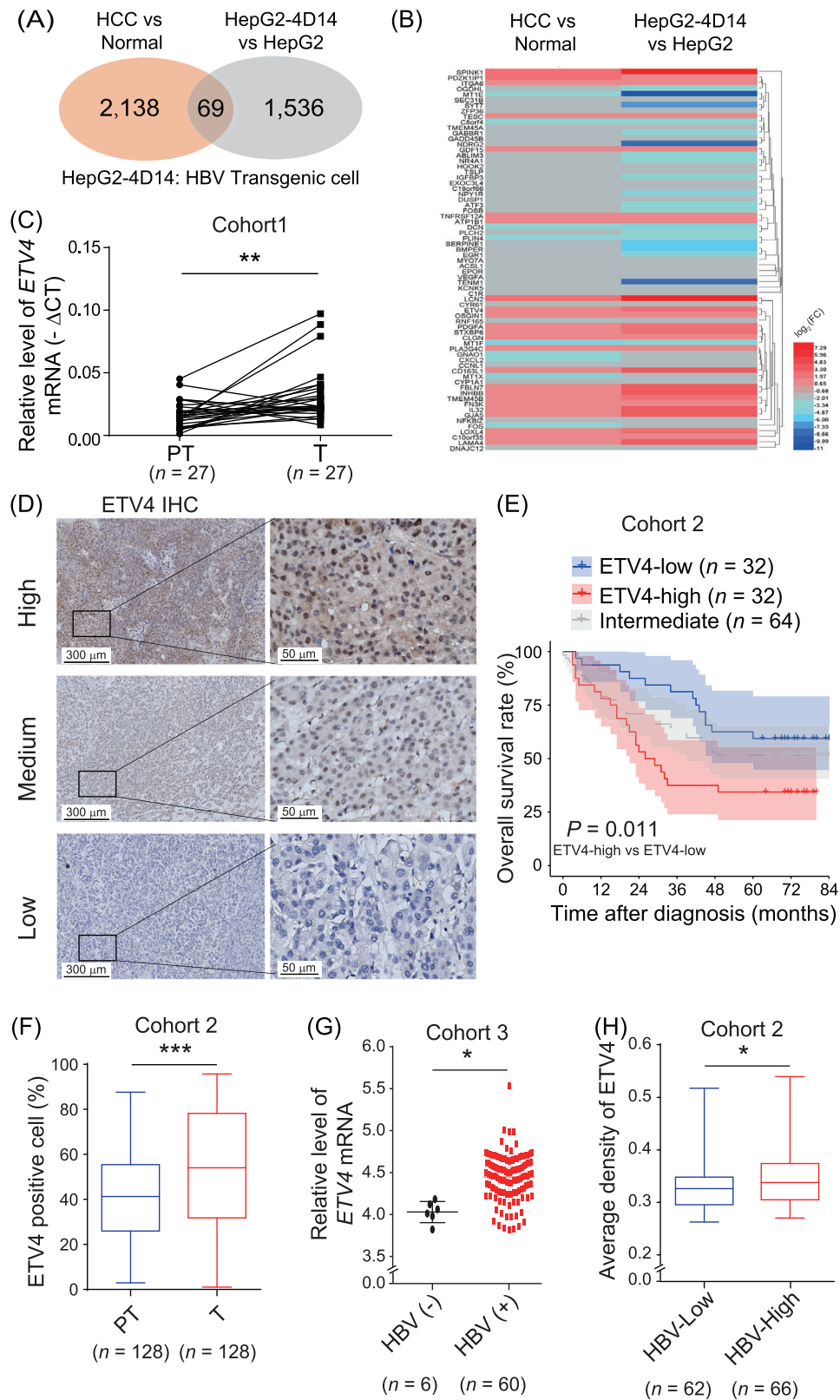


FIGURE 1 *ETV4* is highly expressed in HCC and HBV-positive liver tissues, and its expression is negatively correlated with the survival of HCC patients. (A) Total RNA was extracted from HepG2 and HBV transgenic cell lines HepG2-4D14 and subjected to RNA deep sequencing analysis. The differentially expressed genes in HepG2-4D14 cells compared to HepG2 cells overlapped with the abnormally expressed genes in HCC tumors compared to normal tissues in the TCGA-LIHC cohort. (B) Heatmap of the overlapping genes in A. (C) The *ETV4* level in 27 pairs of HCC tissues and their adjacent nontumoral tissues was determined by qRT-PCR. (D-F) A total of 128 paraffin-embedded primary HCC specimens were subjected to IHC staining with an anti-*ETV4* antibody. The intensity of *ETV4* staining was quantitatively scored with

staining demonstrated that the protein level of ETV4 was higher in tumor tissues from patients with a higher HBV load than in those from patients with a lower HBV load (Figure 1H). These data suggested that the ETV4 level was upregulated in HBV-related HCC.

In addition, we analyzed the TCGA dataset and found that the level of *ETV4* mRNA was also higher in alcohol or non-alcoholic fatty liver disease-associated HCC tumors than in normal tissues (Supplementary Figure S1J).

3.3 | ETV4 directly promoted the transcription of TNF- α and MAPK11

To identify downstream genes regulated by ETV4, we compared the transcription profiles of *ETV4*-overexpressing HepG2 cells (HepG2-*ETV4*-oe) and control cells (HepG2-Ctrl) and *ETV4*-knockdown Huh7 (Huh7-sh*ETV4*) cells and control cells (Huh7-shR) by RNA sequencing. We overlapped the DEGs in the 2 sets described above and identified 159 potential ETV4 downstream genes (Figure 2A-B). By using KEGG pathway analysis, we found that ETV4-upregulated genes were mainly involved in TNF, NF- κ B and MAPK signaling pathways (Figure 2C). TNF- α is an inflammatory cytokine that abnormally expressed in many kinds of chronic or acute liver injury/inflammation [17, 29, 30]. MAPK11 (p38 β) belongs to the family of the p38 MAPKs, which can induce the production of TNF- α and IL-1 β [31–33]. Therefore, TNF- α and MAPK11 were evaluated in priority as they played critical roles in inflammation.

First, we confirmed that *ETV4* knockdown in Huh7 cells caused a reduction in the mRNA levels of TNF- α and *MAPK11* (Figure 2D) as well as the protein level of MAPK11 (Figure 2E). In contrast, overexpression of *ETV4* in HepG2 cells enhanced both the mRNA and protein levels of TNF- α and MAPK11 (Figure 2F-H). We predicted the ETV4-binding sites on the promoters of TNF- α and *MAPK11* on the JASPAR website. Then, we generated the luciferase reporters for the promoters of TNF- α and

MAPK11 and performed luciferase assays. The data showed that ETV4 could significantly enhance the activities of the TNF- α and *MAPK11* promoters (Figure 2I-J). Furthermore, we also performed luciferase assays with the promoters of TNF- α or *MAPK11* in which the potential ETV4-binding sites were mutated, and identified the regions in the TNF- α and *MAPK11* promoters that were critical for ETV4 binding (Figure 2I-J). In addition, we performed the CHIP assay, and the data showed that ETV4 could bind to the promoters of the TNF- α and *MAPK11* directly in Huh7 cells (Figure 2K). In conclusion, ETV4 can directly promote the transcription of TNF- α and *MAPK11*.

3.4 | ETV4 enabled macrophage accumulation and facilitated liver inflammation

To test whether ETV4 could regulate the expression of TNF- α and MAPK11 and enhance the liver inflammation in vivo, we generated hepatocyte-specific *ETV4*-transgenic mice (named as *ETV4*^{Hep-TG}) by crossing *ETV4*^{Rosa26-floxp-gfp-floxp-mETV4/+} mice with Alb-Cre mice (Figure 3A and Supplementary Figure S2A). The genotype of *ETV4*^{Hep-TG} was confirmed by PCR (Supplementary Figure S2B) and ETV4 protein was determined by immunoblotting (Figure 3B). We also generated hepatocyte-specific *ETV4*-knockout mice (*ETV4*^{fl/fl, alb-cre}) by crossing *ETV4*^{fl/fl} with Alb-Cre mice (Figure 3C-D and Supplementary Figure S2C-D). No significant changes of liver/body ratio were observed in 8-week-old *ETV4* transgenic or *ETV4* knockout mice (Supplementary Figure S2E-F).

The protein levels of hepatic TNF- α , MAPK11 and CD68 were examined. The data showed that levels of TNF- α , MAPK11 and CD68 were higher in *ETV4*^{Hep-TG} than that in wild type (WT) mice (Figure 3E-F). To further explore whether ETV4 enhanced the transcription of TNF- α and *MAPK11* in hepatocytes, we isolated primary hepatocytes from the WT or *ETV4*^{Hep-TG} mice, and found that the

the HALO digital pathology system, and samples were classified into three subgroups (high, medium and low) according to their scores. Quartile was used to set the group cutoff. Representative images are shown in D. The overall survival of patients analyzed with Kaplan-Meier analysis is shown in E. The medium was classified as intermediate group. The percentage of ETV4-positive cells in peritumoral and tumor regions in each sample according to IHC staining was calculated by the HALO digital pathology system (F). (G) The relative mRNA level of *ETV4* in HBV-negative ($n = 6$) and HBV-positive ($n = 60$) HCC tissues was measured by qRT-PCR. (H) HCC patients were divided into two groups (HBV-low, $n = 62$; HBV-high, $n = 66$) according to the HBV viral load in their serum. The ETV4 protein levels in HCC tissues were measured by IHC, and the average intensity of ETV4 staining was quantified using the HALO digital pathology system. In the Box and whiskers plots, boxes represented 25-75% percentile, whiskers were min to max, and division line was median. In the scatter plots, division line was mean, whiskers were Standard deviation. * $P < 0.05$, ** $P < 0.01$, *** $P < 0.001$.

Abbreviations: ETV4, ETS translocation variant 4; HBV, hepatitis B virus; HepG2-4D4, HBV Transgenic cell; HCC, hepatocellular carcinoma; TCGA, The Cancer Genome Atlas; LIHC, liver hepatocellular carcinoma; qRT-PCR, real-time quantitative PCR; PT, peritumoral tissue; T, tumor; IHC, immunohistochemistry.

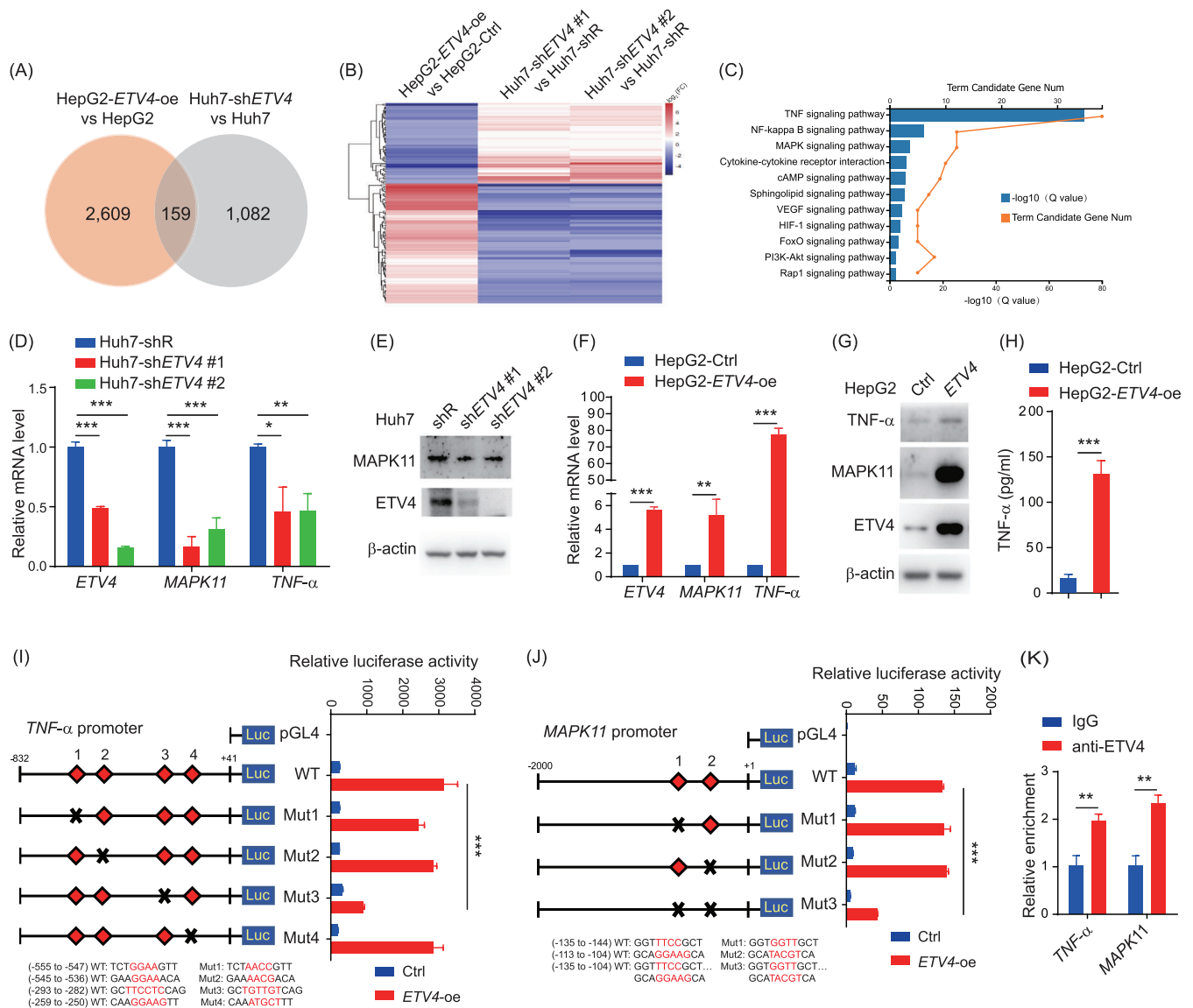


FIGURE 2 ETV4 regulates the transcription of *TNF-α* and *MAPK11*. (A, B) HepG2-ctrl and ETV4-overexpressing HepG2 (HepG2-ETV4-oe), Huh7-shR and ETV4 knockdown Huh7 (shETV4#1, shETV4#2) cells were harvested, and total RNA was extracted and subjected to RNA sequencing. The differentially expressed genes between HepG2 and HepG2-ETV4-oe cells or between Huh7-shR and Huh7-shETV4 cells are shown in a Venn diagram (A) and heatmap (B). (C) KEGG pathway analysis was performed with the genes whose expression levels were upregulated in HepG2-ETV4-oe cells compared to HepG2 cells. (D, E) Total RNA extracted from Huh7-shR, Huh7-shETV4#1, and Huh7-shETV4#2 cells were subjected to qRT-PCR to quantify the mRNA levels of *ETV4*, *MAPK11* and *TNF-α*, three replicates were performed (D). The protein levels of ETV4 and MAPK11 in the cells mentioned above were determined by immunoblotting with actin as the internal control, two replicates were performed (E). (F-H) Total RNA extracted from HepG2-ctrl and HepG2-ETV4-oe cells was subjected to qRT-PCR to measure the mRNA levels of *ETV4*, *MAPK11* and *TNF-α*, three replicates were performed (F). TNF-α and MAPK11 protein levels in the cells mentioned above were measured by immunoblotting with the indicated antibodies, three replicates were performed (G). TNF-α levels in the supernatant were measured by ELISA, four replicates were performed (H). (I) 293T cells were transfected with pLL-ETV4 and the *TNF-α* promoter luciferase reporter (WT) or a luciferase reporter with the potential ETV4 binding sites mutated (Mut1-4) for 24 h. The cell lysates were harvested and subjected to luciferase assay. Two replicates were performed. (J) 293T cells were transfected with pLL-ETV4 and the *MAPK11* promoter luciferase reporter (WT) or a luciferase reporter with the potential ETV4 binding sites mutated (Mut1-3) for 24 h. The cell lysates were harvested and subjected to luciferase assay. Three replicates were performed. (K) CHIP assay was performed in Huh7 cells with anti-ETV4 antibodies or anti-IgG control. qRT-PCR was used to quantify the relative fold change of ETV4 on *TNF-α* or *MAPK11* promoter. Two replicates were performed. The column bar graphs were presented as the mean ± SD. * *P* < 0.05, ** *P* < 0.01, *** *P* < 0.001.

Abbreviations: ETV4, ETS translocation variant 4; TNF-α, tumor necrosis factor alpha; MAPK11, mitogen-activated protein kinase 11; oe, overexpression; shR, control shRNA; Ctrl, control; WT, wild type; Mut, mutation; ELISA, enzyme-linked immunosorbent assay; CHIP, chromatin immunoprecipitation; qRT-PCR, real-time quantitative PCR; Luc, luciferase.

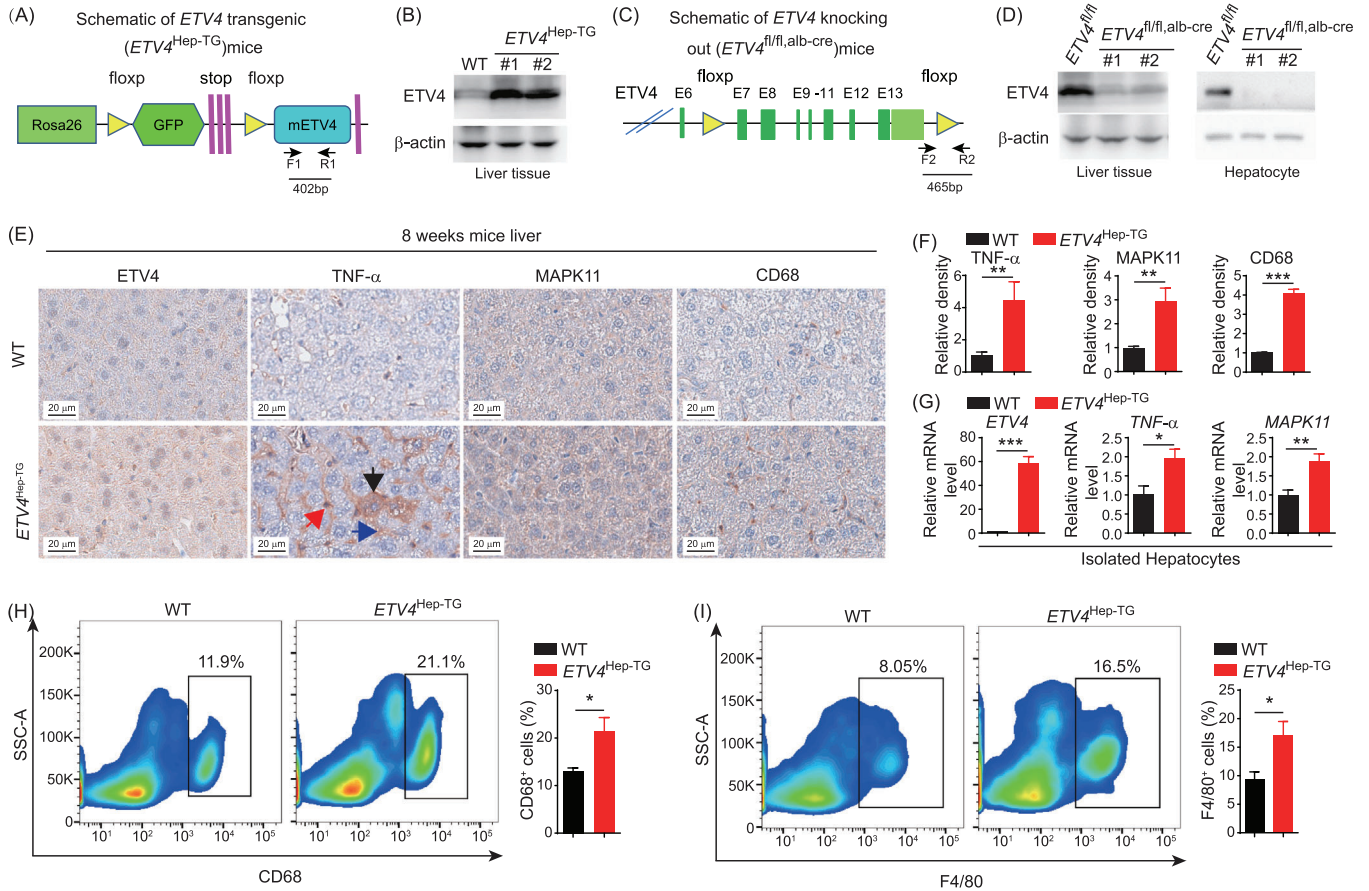


FIGURE 3 ETV4 upregulates TNF- α /MAPK11 expression and liver inflammation. (A) The genomic map of conditional *ETV4*-transgenic mice (*ETV4*^{Rosa26-floxp-gfp-floxp-mETV4/+}). The F1 and R1 primers were used for genotyping. (B) *ETV4*^{Rosa26-floxp-gfp-floxp-mETV4/+} mice were crossed with hepatocyte-specific Cre mice to generate *ETV4*^{Hep-TG} (*ETV4*^{Rosa26-floxp-gfp-floxp-mETV4/+; alb-cre}) mice. The cell lysates from liver tissues of 8-week-old WT or *ETV4*^{Hep-TG} mice were subjected to immunoblotting with an anti-ETV4 antibody. (C) The genomic map of conditional *ETV4*-knockout mice (*ETV4*^{fl/fl, alb-cre}); F2 and R2 represent the primers used for genotyping. (D) The lysates from the total liver tissues (left) and hepatocyte isolated by perfusion (right) of 8-week-old *ETV4*^{fl/fl} or *ETV4*^{fl/fl, alb-cre} mice were subjected to immunoblotting with an anti-ETV4 antibody. (E, F) WT (*n* = 5) or *ETV4*^{Hep-TG} (*n* = 3) mice were sacrificed at 8 weeks of age, and liver tissues were harvested and subjected to IHC staining of TNF- α , MAPK11 and CD68. Representative images are shown (E). Black arrow, TNF- α positive hepatocyte; Blue arrow, TNF- α in intracellular area; Red arrow, TNF- α positive immune cell. The intensity of TNF- α , MAPK11 and CD68 staining was quantified (F). (G) Hepatocytes were isolated from WT (*n* = 7) or *ETV4*^{Hep-TG} (*n* = 8) mice. The relative mRNA level of *ETV4*, *TNF- α* and *MAPK11* were determined by qRT-PCR. (H, I) The proportions of CD68⁺ (H) and F4/80⁺ (I) cells were analyzed by flow cytometry in 8-week-old WT and *ETV4*^{Hep-TG} mice liver. The column bar graphs were presented as the mean \pm SD. * *P* < 0.05, ** *P* < 0.01, *** *P* < 0.001. Abbreviations: ETV4, ETS translocation variant 4; TNF- α , tumor necrosis factor alpha; MAPK11, mitogen-activated protein kinase 11; WT, wild type; Alb-Cre, cre driven by albumin promoter; IHC, immunohistochemistry; qRT-PCR, real-time quantitative PCR.

mRNA levels of *TNF- α* and *MAPK11* in hepatocytes were significantly higher in *ETV4*^{Hep-TG} than that in WT mice (Figure 3G). We further performed the flow cytometry analysis and found that both CD68⁺ and F4/80⁺ cells were significantly enriched in *ETV4*^{Hep-TG} than in WT mice (Figure 3H-I). The neutrophils were also higher in *ETV4*^{Hep-TG} mice than in WT mice, but there was no difference of CD4⁺ T cells and CD8⁺ T cells between WT and *ETV4*^{Hep-TG} mice (Supplementary Figure S3). Taken together, these results indicated that ETV4 promoted the expression of TNF- α and MAPK11 in hepatocytes and

the accumulation of macrophages and neutrophils in the liver.

To investigate whether ETV4 promoted the expression of TNF- α and MAPK11 and the accumulation of macrophages during liver inflammation, we measured the protein levels of TNF- α , MAPK11 and CD68 in the livers of control mice and mice treated with DEN to induce acute inflammation and found that TNF- α , MAPK11 and CD68 were expressed higher in the *ETV4*^{Hep-TG} mice than in the WT mice (Figure 4A-B). We also performed macrophage depletion with GdCl₃ in mice treated with DEN and found that

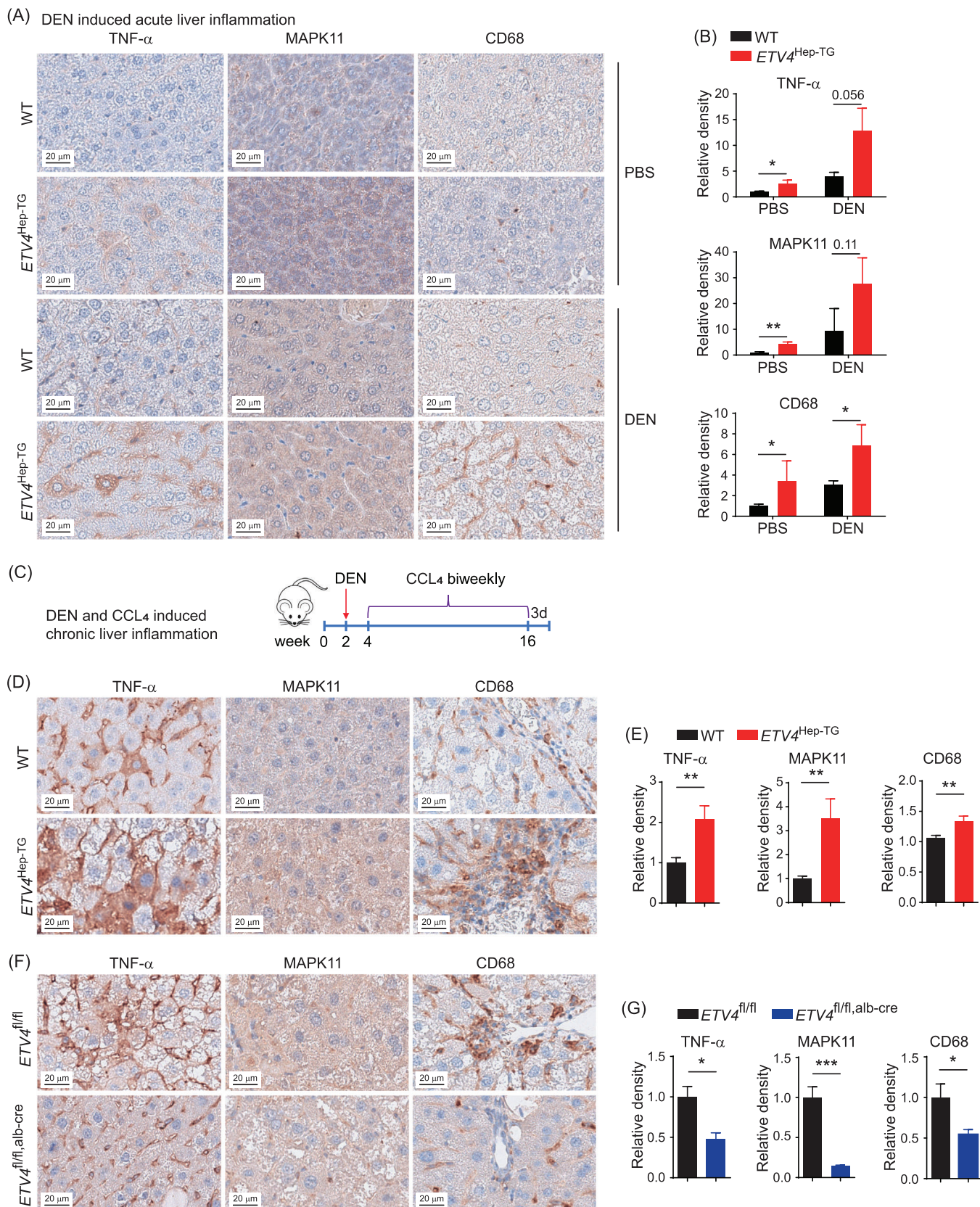


FIGURE 4 *ETV4* enhances macrophage accumulation and inflammation in liver under injury. (A, B) Eight-week-old WT or *ETV4*^{Hep-TG} mice were intraperitoneally injected with DEN (100 mg/kg) or PBS for 8 h, and the livers were harvested and subjected to IHC staining to measure the protein levels of TNF- α , MAPK11 and CD68 (A). The intensities of the proteins mentioned above were calculated (B). WT PBS ($n = 4$), *ETV4*^{Hep-TG} PBS ($n = 4$), WT DEN ($n = 4$), *ETV4*^{Hep-TG} DEN ($n = 4$). (C) Schematic of DEN-CCL₄ induced chronic liver inflammation in mice. (D-G) Wild-type and *ETV4*^{Hep-TG} or *ETV4*^{fl/fl} and *ETV4*^{fl/fl,alb-cre} mice were treated as shown in C. The liver tissues were harvested from

TNF- α expression was still higher in *ETV4*^{Hep-TG} than in WT mice (Supplementary Figure S4A-B). The above data indicated that *ETV4* could upregulate TNF- α expression and enhance macrophage accumulation in the liver during acute inflammation. To uncover the effect of *ETV4* during chronic liver injury and inflammation, we treated the mice with DEN combined with CCL₄ (Figure 4C). IHC staining showed that the levels of TNF- α , MAPK11 and CD68 in the livers of the *ETV4*^{Hep-TG} mice were higher than those in WT mice (Figure 4D-E), indicating that *ETV4* could trigger liver inflammation and macrophage accumulation via upregulating TNF- α and MAPK11 expression when there was chronic liver injury. Otherwise, knockout of *ETV4* caused a marked reduction in the TNF- α , MAPK11 and CD68 levels (Figure 4F-G). To completely exclude the possible influence of acute liver injury caused by CCL₄, we further measured the protein levels of TNF- α , MAPK11 and CD68 in the liver samples from the mice 7 days after the final injection of CCL₄ (Supplementary Figure S4C) and obtained consistent results in the *ETV4*^{Hep-TG} mice (Supplementary Figure S4D-E) and the *ETV4*^{fl/fl, alb-cre} mice (Supplementary Figure S4F-G). Overall, these results demonstrated that *ETV4* enabled macrophage accumulation and facilitated liver inflammation via modulating the *ETV4*-TNF- α and *ETV4*-MAPK11 axis.

The data showed that *ETV4* could promote the inflammation in the liver. In order to know whether inflammation could influence the level of *ETV4*, we treated the mice with DEN or CCL₄, and observed that the mRNA level of *ETV4* in the liver was increased after treatment with DEN or CCL₄ (Supplementary Figure S5), indicating that inflammation may also trigger the transcription of *ETV4*.

3.5 | *ETV4* promoted liver tumorigenesis

Chronic inflammation plays an important role in HCC development. To identify whether *ETV4* could promote liver tumorigenesis in vivo, we established the DEN-CCL₄-treated HCC model in transgenic mice (Figure 5A). After DEN-CCL₄ treatment, the number of total surface tumors and the number of tumors larger than 1 mm³ were lower in the livers of the *ETV4*^{fl/fl, alb-cre} mice than in those of the *ETV4*^{fl/fl} mice (Figure 5B-D), and the liver/body weight

ratio was also lower in the *ETV4*^{fl/fl, alb-cre} mice than in the *ETV4*^{fl/fl} mice (Figure 5E). In addition, the number of microscopic tumors in the *ETV4*^{fl/fl, alb-cre} mice were lower than that in the *ETV4*^{fl/fl} mice (Figure 5F-H). These data indicated that knockout of *ETV4* in hepatocytes suppressed liver tumor formation in DEN-CCL₄ HCC model.

A DEN-CCL₄ HCC model with *ETV4*^{Hep-TG} mice was also established (Figure 5I). Total number of surface tumors in the livers of the *ETV4*^{Hep-TG} mice was higher than those in the WT mice (Figure 5J-K). No significant difference was observed in the number of surface tumors larger than 1 mm³ and the liver/body ratio between the *ETV4*^{Hep-TG} and WT mice (Figure 5L-M), but total numbers of microscopic tumors and the numbers of large microscopic tumors were robust higher in the *ETV4*^{Hep-TG} mice than in the WT mice (Figure 5N-P). All these data suggested that *ETV4* promoted HCC formation and could be a potential therapeutic target for HCC. In addition, the protein levels of TNF- α , MAPK11 and CD68 were lower in the liver tissues of the *ETV4*^{fl/fl, alb-cre} mice than in those of the *ETV4*^{fl/fl} mice (Figure 5Q-R) and significantly higher in the *ETV4*^{Hep-TG} mice than in the WT mice (Figure 5S-T), suggesting that *ETV4* promoted the expression of TNF- α and MAPK11 and hepatic macrophage infiltration during the development of DEN-CCL₄-induced HCC.

3.6 | *ETV4* expression was positively correlated with TNF- α and MAPK11 expression and liver inflammation in human HCC samples

As shown in Figure 1C and Supplementary Figure S1C-F, the level of *ETV4* was higher in HCC tumors than in adjacent peritumoral tissues. If *ETV4* promoted liver tumorigenesis through TNF- α and MAPK11, there should be higher levels of TNF- α and MAPK11 in tumor tissues than in peritumoral tissues. As expected, there were more TNF- α - and MAPK11-positive cells and higher H-scores of TNF- α and MAPK11 in tumors than in peritumoral tissues according to the IHC staining results of Cohort 2 (Figure 6A-D, Supplementary Figure S6). TNF- α and MAPK11 expression were also higher in tissues with high *ETV4* expression than in tissues with low *ETV4* expression

the sacrificed mice and subjected to IHC staining for TNF- α , MAPK11 and CD68. Representative images are shown in D, F. The intensities of TNF- α , MAPK11 and CD68 staining were quantified (E, G). WT ($n = 8$), *ETV4*^{Hep-TG} ($n = 8$), *ETV4*^{fl/fl} ($n = 5$), *ETV4*^{fl/fl, alb-cre} ($n = 7$). The column bar graphs were presented as the mean \pm SD. * $P < 0.05$, ** $P < 0.01$, *** $P < 0.001$.

Abbreviations: *ETV4*, ETS translocation variant 4; TNF- α , tumor necrosis factor alpha; MAPK11, mitogen-activated protein kinase 11; DEN, diethylnitrosamine; PBS, phosphate buffered saline; WT, wild type; Alb-Cre, cre driven by albumin promoter; CCL₄, carbon tetrachloride; IHC, immunohistochemistry.

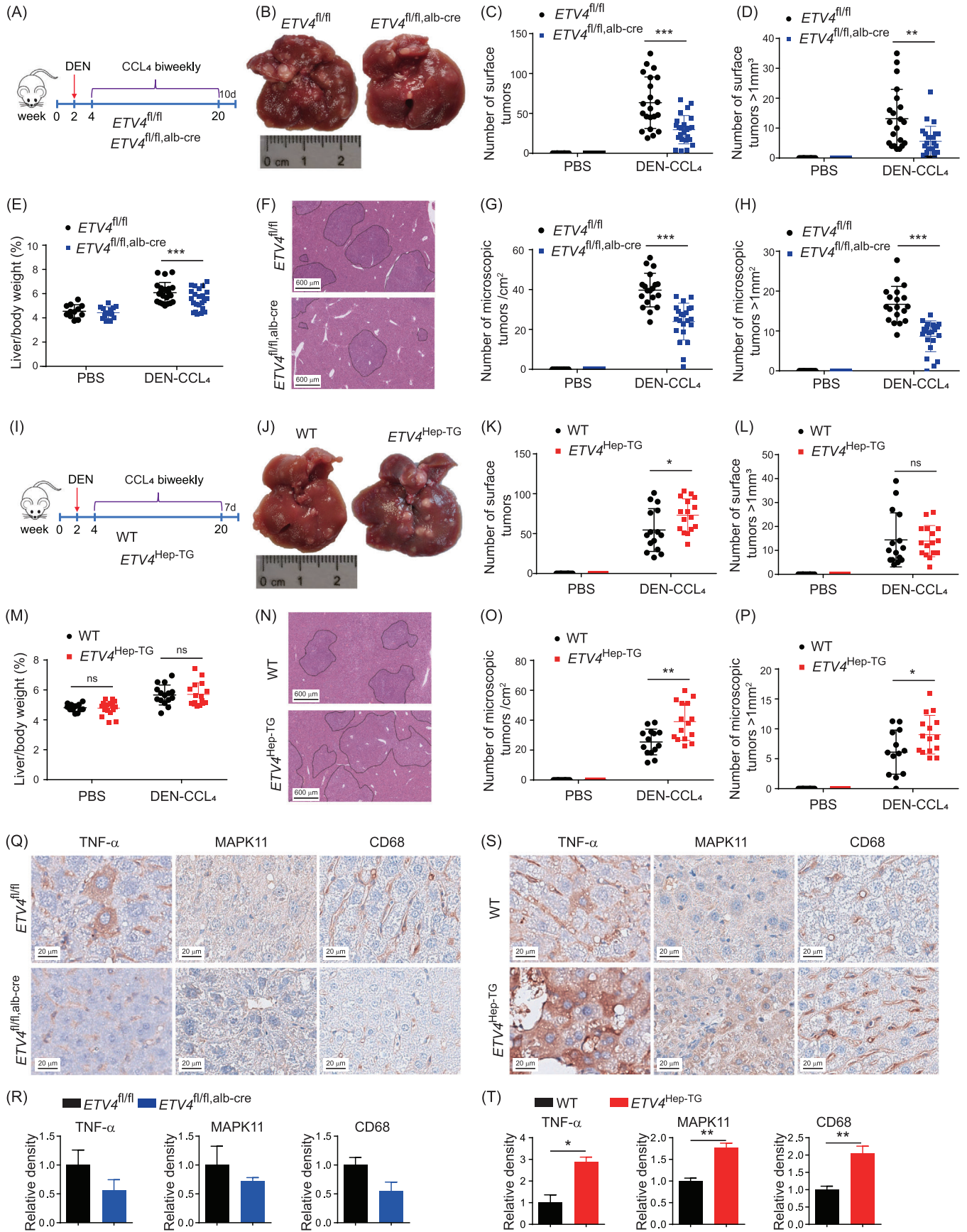


(Figure 6E). Then the mRNA levels of *ETV4*, *TNF-α* and *MAPK11* in the HCC tumors in Cohort 3 were analyzed by qRT-PCR. The data showed that *ETV4* expression was positively correlated with *TNF-α* and *MAPK11* expression (Figure 6F-G). By analyzing the HCC single-cell transcriptome data from public database, we further found that *ETV4* was mainly expressed in tumor cells (Figure 6H), and *TNF-α* and *MAPK11* were co-expressed with *ETV4* in tumor cells (Figure 6I-J). We divided the patients in Cohort 2 into different groups according to the levels of *TNF-α*, *MAPK11* and *ETV4* and performed Kaplan-Meier survival analysis. The results demonstrated that patients with higher *TNF-α* level had poorer survival than those with lower *TNF-α* level (Figure 6K), while the OS had no significant difference between patients with higher *MAPK11* and those with lower *MAPK11* (Figure 6L). Furthermore, patients with higher levels of *ETV4*+*TNF-α* had an even worse survival rate than those with lower levels of *ETV4*+*TNF-α* (Figure 6M), while patients with higher levels of *ETV4*+*MAPK11* had poorer survival rate than those with lower levels of *ETV4*+*MAPK11* (Figure 6N). These data suggested that *ETV4*+*TNF-α* might be used as prognostic markers for HCC patients. We analyzed the correlation of *ETV4* level in tumor with the scores of immune cell types enumerated by xCell, and found that there were more monocytes (Figure 6O) and macrophages (Figure 6P) in *ETV4*-high tumors than that in *ETV4*-low tumors, indicating more monocyte and macrophage infiltration in *ETV4*-high tumors.

Taken together, our data suggested that *ETV4* promoted liver inflammation and tumorigenesis via enhancing the *TNF-α* and *MAPK11* signaling pathway (Figure 7).

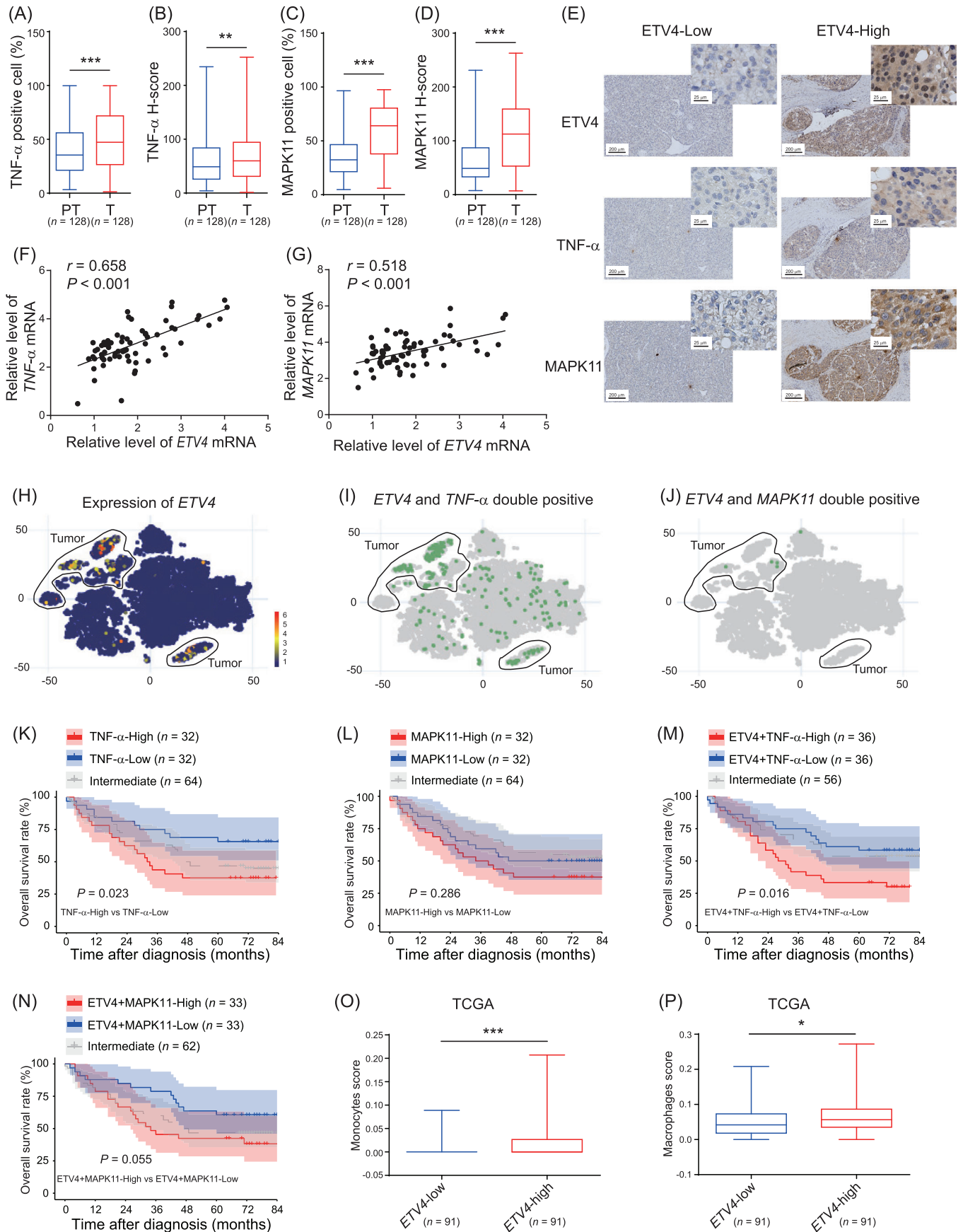
4 | DISCUSSION

In the present study, we found that *ETV4* in hepatocytes could promote the inflammation and macrophage accumulation in the liver of mice. Overexpression of *ETV4* (*ETV4*^{Hep-TG}) promoted the HCC formation in mice, while knockout of *ETV4* (*ETV4*^{fl/fl, alb-cre}) inhibited the HCC formation. *ETV4* promoted the transcription of *TNF-α* and *MAPK11* both in vitro and in vivo. The *ETV4*+*TNF-α* level was negatively correlated with the survival of HCC patients.

As a transcription factor, *ETV4* was shown to promote the development of different kinds of cancer by increasing cell proliferation and metastasis. *ETV4* directly regulated the transcription of matrix metalloproteinase 13 (MMP13) and promoted the invasion and metastasis of breast cancer [34]. *ETV4* also downregulated Cyclin-dependent kinase inhibitor 1A (CDKN1A) expression by binding to the promoter of CDKN1A and increased the proliferation of prostate cancer cells [35]. In addition, *ETV4* facilitated Yes-associated protein (YAP)/TEA domain family member (TEAD)-mediated transcriptional activation and enhanced the progression of HCC [36], and regulated the expression of MMP family members to promote tumor metastasis [34, 37, 38]. In this study, we revealed that *ETV4* promoted HCC development by regulating liver inflammation via the *TNF-α* pathway.

TNF-α is an inflammatory cytokine which is abnormally expressed in the liver during damage, and it plays a key role in HCC development. For instance, *TNF-α* expression was upregulated during DEN- or CCL₄-induced acute liver damage [39]. *TNF-α* expression was enhanced under the conditions of HFD-, choline-deficient and

FIGURE 5 *ETV4* promotes DEN-CCL₄-induced HCC formation. (A) Schematic of DEN-CCL₄-induced HCC in *ETV4*^{fl/fl} and *ETV4*^{fl/fl, alb-cre} mice. (B-H) The liver tissues from sacrificed mice as shown in A were harvested. Representative images of the livers of *ETV4*^{fl/fl} and *ETV4*^{fl/fl, alb-cre} mice are shown (B). The total number of surface tumors and the number of surface tumors larger than 1 mm³ were calculated (C, D). The liver/body weight of the mice was measured (E). The livers were fixed and subjected to H&E staining. Representative images are shown (F). The total number of microscopic tumors per cm² and the number of microscopic tumors larger than 1 mm² per cm² were calculated according to the H&E staining in F (G, H). *ETV4*^{fl/fl} PBS (*n* = 12), *ETV4*^{fl/fl, alb-cre} PBS (*n* = 14), *ETV4*^{fl/fl} DEN (*n* = 21), *ETV4*^{fl/fl, alb-cre} DEN (*n* = 24). (I-P) Schematic of DEN- and CCL₄-induced HCC in WT and *ETV4*^{Hep-TG} mice (I). The mice were sacrificed at the indicated times, and the livers were harvested. Representative images of the livers of WT and *ETV4*^{Hep-TG} mice are shown (J). The number of surface tumors and the number of surface tumors larger than 1 mm³ were calculated (K, L). The liver/body weight of the mice was measured (M). The livers were fixed and subjected to H&E staining, and representative images are shown (N). The total number of microscopic tumors per cm² and the number of microscopic tumors larger than 1 mm² per cm² were calculated according to the H&E staining in N (O, P). WT PBS (*n* = 12), *ETV4*^{Hep-TG} PBS (*n* = 17), WT DEN (*n* = 15), *ETV4*^{Hep-TG} DEN (*n* = 16). (Q-T) The DEN-CCL₄-induced HCC in *ETV4*^{fl/fl} and *ETV4*^{fl/fl, alb-cre} or WT and *ETV4*^{Hep-TG} mice were sacrificed, the livers of mice were subjected to IHC staining for *TNF-α*, *MAPK11* and CD68. Representative images are shown in Q and S. The intensities of *TNF-α*, *MAPK11* and CD68 staining were quantified in R and T. *ETV4*^{fl/fl} (*n* = 3), *ETV4*^{fl/fl, alb-cre} (*n* = 3), WT (*n* = 3), *ETV4*^{Hep-TG} (*n* = 3). The column bar graphs were presented as the mean ± SD. In the scatter plots, division line was mean, whiskers were Standard deviation. * *P* < 0.05, ** *P* < 0.01, *** *P* < 0.001, ns, not statistically significant. Abbreviations: *ETV4*, ETS translocation variant 4; *TNF-α*, tumor necrosis factor alpha; *MAPK11*, mitogen-activated protein kinase 11; DEN, diethylnitrosamine; PBS, phosphate buffered saline; d, days; WT, wild type; Alb-Cre, cre driven by albumin promoter; CCL₄, carbon tetrachloride; H&E, hematoxylin and eosin staining; IHC, immunohistochemistry.



ethionine-supplemented (CDE) diet- or CCL₄-induced chronic liver injury [21]. TNF- α expression was also elevated in the livers with hepatic dysfunction, such as cholestasis [20, 40]. Loss of TNFR1 reduced the liver tumorigenesis induced by DEN and HFD [18]. Depletion of TNFR1 inhibited HCC development in MUP-uPA mice, which had high urokinase plasminogen activator (uPA) expression [40]. Our findings revealed that ETV4 promoted the expression of TNF- α and enhanced tumor formation. It is possible that interference of TNF- α or TNFR1 may reduce tumorigenesis induced by ETV4 overexpression.

It had been reported that the inflammatory cytokines IL-6, TNF- α , IL-1 β and lymphotoxin-A accelerated the development and aggressiveness of HCC in a mouse model [14–18]. Previous studies had revealed that TNF- α was mainly produced by non-hepatocytes in *mdr2*^{-/-} mice [20] and was mostly secreted by inflammatory cells during CDE diet-induced liver inflammation [21]. In this study, we surprisingly found that ETV4 promoted the transcription of TNF- α in hepatocytes and led to the higher level of TNF- α in the liver, which induced inflammation and promoted tumorigenesis. It would be worth to further investigate the function of hepatocyte-secreted TNF- α in tumor microenvironment and the transition of chronic inflammation to tumor.

A previous study reported that ETV4 could promote the transcription of C-X-C motif chemokine ligand 1 (CXCL1) and CXCL5 in HCC cells and led to the changes of immune cells in the subcutaneous tumors [36]. However, whether the phenotype obtained from the subcutaneous tumor model would truly occur under the physiological condition needed further investigation. By using orthotopic

xenograft models, Xie et al. [41] found that ETV4 upregulated the transcription of programmed cell death-ligand 1 (PD-L1) and C-C motif chemokine ligand 2 (CCL2) and promoted HCC metastasis. Their results may represent the microenvironment in late stage during tumor development since they performed the experiments with the tumor cell line Hepa1-6. In the present study, we found that ETV4 enhanced the inflammation and tumorigenesis by promoting the transcription of TNF- α and MAPK11 in hepatocyte-specific *ETV4*^{Hep-TG} and *ETV4*^{fl/fl, alb-cre} mice. These data implied that ETV4 played an important role in inflammation-tumor transition at the early stage of tumor formation, suggesting that ETV4 could affect multiple signaling pathways at different stages of HCC development.

HBV is one of the risk factors that induces chronic hepatitis. Other types of hepatitis are observed in the clinic, such as NASH, alcoholic steatohepatitis and cholestasis-induced hepatitis [2, 4]. The present study indicated that HBV induced the expression of ETV4, which promoted liver tumorigenesis. In addition, we found that ETV4 was upregulated in alcohol assumption- and non-alcoholic fatty liver disease-associated HCC compared to normal livers. We also observed that the level of *ETV4* mRNA was increased in the livers of mice treated with DEN or CCL₄. These data indicated that inflammation could also trigger the transcription of *ETV4*. It suggested that inflammation and ETV4 formed positive feedback. If so, it is possible that ETV4 also plays a critical role during the development of inflammation-related liver diseases other than HCC.

Previous studies showed that the monocyte-derived macrophages played an important role during the HCC development [42–44]. Our data showed that there was more macrophage accumulation in *ETV4*^{Hep-TG} mice.

FIGURE 6 ETV4 expression is significantly correlated with TNF- α and MAPK11 expression in liver tissues of HCC patients. (A–D) A total of 128 paraffin-embedded liver tissues from HCC patients were subjected to IHC staining for TNF- α and MAPK11. The numbers of TNF- α - and MAPK11-positive cells in the peritumoral (PT) and tumoral (T) tissues were calculated using the HALO digital pathology system. The proportion of TNF- α - and MAPK11-positive cells are shown in A and C. The H-scores of TNF- α and MAPK11 are shown in B and D. H-score = weak positive cell percentage \times 1 + moderately positive cell percentage \times 2 + strongly positive cell percentage \times 3. (E) IHC staining of ETV4, TNF- α and MAPK11 were performed in Cohort 2. The samples were subclassified into ETV4-High or ETV4-Low groups according to the average intensity of ETV4, the presentative images of TNF- α and MAPK11 in ETV4-High or -Low groups were shown in E. (F, G) HCC samples from 66 HCC patients (Cohort 3) were collected, and total RNA was extracted and subjected to qRT-PCR to determine the mRNA levels of *ETV4*, *TNF- α* and *MAPK11*. The Pearson correlation coefficient (*r*) and *P* value of *ETV4* with *TNF- α* or *ETV4* with *MAPK11* were analyzed. (H–J) The expression of *ETV4* (H) and the double positive of *ETV4* with *TNF- α* (I) or *ETV4* with *MAPK11* (J) were analyzed based on the scRNA-seq of HCC tumor specimens (<https://db.cngb.org/PRHCCdb/>). (K–N) Based on the IHC staining for ETV4, MAPK11 and TNF- α from cohort 2, the average intensity of the staining for those proteins was analyzed using a HALO digital pathology system. The samples were classified into high and low groups for TNF- α , MAPK11, ETV4+TNF- α , or ETV4+MAPK11. The Kaplan-Meier overall survival of patients in different groups was analyzed. (O–P) The cell subsets were enumerated by xCell (<https://comphealth.ucsf.edu/app/xcell>) based on LIHC RNA-seq data in TCGA. The monocytes (O) and macrophage (P) score was shown in *ETV4*-low and *ETV4*-high groups. *ETV4*-low and -high were classified in quartile according to the *ETV4* level in TCGA LIHC. In the Box and whiskers plots, boxes represented 25–75% percentile, whiskers were min to max, and division line was median. * *P* < 0.05, ** *P* < 0.01, *** *P* < 0.001. Abbreviations: ETV4, ETS translocation variant 4; TNF- α , tumor necrosis factor alpha; MAPK11, mitogen-activated protein kinase 11; PT, peritumoral tissue; T, tumor; HCC, hepatocellular carcinoma; scRNA-seq, single cell RNA sequencing; LIHC, liver hepatocellular carcinoma; TCGA, The Cancer Genome Atlas; IHC, immunohistochemistry; qRT-PCR, real-time quantitative PCR.

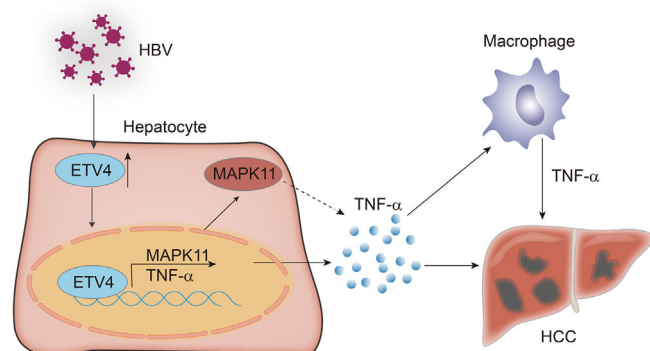


FIGURE 7 The model of ETV4 promoted liver inflammation and tumorigenesis. ETV4 was upregulated by HBV infection, the upregulation of ETV4 promote the hepatocyte released TNF- α and hepatic TNF- α secretion, thus facilitated macrophages accumulation and promoted tumorigenesis.

Abbreviations: ETV4, ETS translocation variant 4; HBV, hepatitis B virus; TNF- α , tumor necrosis factor alpha; MAPK11, mitogen-activated protein kinase 11.

However, we did not examine whether the macrophage enhancement in *ETV4*^{Hep-TG} mice was from monocyte differentiation or Kupffer cell proliferation, which needed further investigation. In addition, the functions of different subpopulations of macrophages were divergent during HCC development [22, 45, 46]. Therefore, it is worthwhile to further explore which subpopulation of macrophage is affected by ETV4 to better understand the function of ETV4 in inflammation and HCC formation. We also observed more neutrophil accumulation in *ETV4*^{Hep-TG} mice. It has been reported that N2 neutrophils promoted tumor formation by enhancing reactive oxygen species [47]. It will be worth to study what type of neutrophils was accumulated in *ETV4*^{Hep-TG} mice in the future.

5 | CONCLUSIONS

In conclusion, we found that ETV4 was highly expressed in HCC, and its expression was negatively associated with the survival of HCC patients. ETV4 promoted liver inflammation and enhanced liver tumorigenicity in vivo. Mechanistically, ETV4 could promote the transcription of TNF- α and MAPK11 directly, and enhanced liver inflammation by increasing macrophages and neutrophils. We demonstrated that the level of ETV4+TNF- α was negatively associated with the survival of HCC patients, which may be potential prognostic markers for HCC patients.

DECLARATIONS

AUTHOR CONTRIBUTIONS

Dandan Qi and Min Lu designed and performed the experiments, and wrote the draft. Pengfei Xu performed the IHC

staining. Xinli Yao, Yongchen Chen, Yahua Cui and Lipeng Gan supported the mouse experiments. Yong Li performed the statistical analysis. Xiaomei Tong and Shuhong Liu contributed to the constructive discussions. Jingmin Zhao provided the clinical samples and contributed to the constructive discussions. Ningning Liu interpreted data and revised the manuscript. Xin Ye supervised the study and wrote the manuscript.

ACKNOWLEDGMENTS

We are grateful to Xiaolan Zhang, Meng Wan and Xiaopeng Yang for providing technical support for the IHC staining analysis. We are also grateful to Nanjing Freethinking Biotechnology Co., Ltd. (China) for providing HALO pathology analysis services.

CONFLICT OF INTEREST STATEMENT

The authors declare no conflict of interest.

CONSENT FOR PUBLICATION

Not applicable.

DATA AVAILABILITY STATEMENT

The overall survival of ETV4 in TCGA was from GEPIA (<http://gepia.cancer-pku.cn/>). The gene expression profiles were from TCGA datasets (<https://www.cancer.gov/ccg/research/genome-sequencing/tcga>), the Gene Omnibus database (GEO) was from NCBI (GEO DataSets - NCBI (nih.gov)). The immune cell enrichment profiles were from xCell (<https://xcell.ucsf.edu/>). The quantitative form of IHC staining in Cohort 2 by HALO digital platform are available from the corresponding author for reasonable request.

ETHICS APPROVAL AND CONSENT TO PARTICIPATE

The HCC tissues in Cohorts 1-3 were all from the Fifth Medical Center of Chinese PLA General Hospital. This study was approved by the Ethics Committee of the Fifth Medical Center of Chinese PLA General Hospital (GH-7-20180563). All the experiments were performed according to approved guidelines and regulations. Animal studies were approved by Institute of Microbiology, Chinese Academy of Sciences, Research Ethics Committee and were performed according to the application guidelines and regulations (APIMCAS2019009).

ORCID

Xin Ye  <https://orcid.org/0000-0001-5217-940X>

REFERENCES

- Sung H, Ferlay J, Siegel RL, Laversanne M, Soerjomataram I, Jemal A, et al. Global Cancer Statistics 2020: GLOBOCAN

- Estimates of Incidence and Mortality Worldwide for 36 Cancers in 185 Countries. *CA Cancer J Clin.* 2021;71(3):209–49.
2. Ringelhan M, Pfister D, O'Connor T, Pikarsky E, Heikenwalder M. The immunology of hepatocellular carcinoma. *Nat Immunol.* 2018;19(3):222–32.
 3. Forner A, Reig M, Bruix J. Hepatocellular carcinoma. *Lancet.* 2018;391(10127):1301–14.
 4. Villanueva A. Hepatocellular Carcinoma. *N Engl J Med.* 2019;380(15):1450–62.
 5. Muller M, Bird TG, Nault JC. The landscape of gene mutations in cirrhosis and hepatocellular carcinoma. *J Hepatol.* 2020;72(5):990–1002.
 6. Wangenstein KJ, Chang KM. Multiple Roles for Hepatitis B and C Viruses and the Host in the Development of Hepatocellular Carcinoma. *Hepatology.* 2021;73 Suppl 1:27–37.
 7. Qiu H, Cao S, Xu R. Cancer incidence, mortality, and burden in China: a time-trend analysis and comparison with the United States and United Kingdom based on the global epidemiological data released in 2020. *Cancer Commun (Lond).* 2021;41(10):1037–48.
 8. Li W, Yang L, He Q, Hu C, Zhu L, Ma X, et al. A Homeostatic Arid1a-Dependent Permissive Chromatin State Licenses Hepatocyte Responsiveness to Liver-Injury-Associated YAP Signaling. *Cell Stem Cell.* 2019;25(1):54–68 e5.
 9. Gadd VL, Aleksieva N, Forbes SJ. Epithelial Plasticity during Liver Injury and Regeneration. *Cell Stem Cell.* 2020;27(4):557–73.
 10. Lefere S, Van de Velde F, Hoorens A, Raevens S, Van Campenhout S, Vandierendonck A, et al. Angiopoietin-2 Promotes Pathological Angiogenesis and Is a Therapeutic Target in Murine Nonalcoholic Fatty Liver Disease. *Hepatology.* 2019;69(3):1087–104.
 11. Sangro B, Sarobe P, Hervas-Stubbs S, Melero I. Advances in immunotherapy for hepatocellular carcinoma. *Nat Rev Gastroenterol Hepatol.* 2021;18(8):525–43.
 12. Yang LY, Luo Q, Lu L, Zhu WW, Sun HT, Wei R, et al. Increased neutrophil extracellular traps promote metastasis potential of hepatocellular carcinoma via provoking tumorous inflammatory response. *J Hematol Oncol.* 2020;13(1):3.
 13. Lee JW, Stone ML, Porrett PM, Thomas SK, Komar CA, Li JH, et al. Hepatocytes direct the formation of a pro-metastatic niche in the liver. *Nature.* 2019;567(7747):249–52.
 14. Grivnennikov SI, Karin M. Inflammatory cytokines in cancer: tumour necrosis factor and interleukin 6 take the stage. *Ann Rheum Dis.* 2011;70 Suppl 1:i104–8.
 15. He G, Karin M. NF-kappaB and STAT3 - key players in liver inflammation and cancer. *Cell Res.* 2011;21(1):159–68.
 16. Maeda S, Kamata H, Luo JL, Leffert H, Karin M. IKKbeta couples hepatocyte death to cytokine-driven compensatory proliferation that promotes chemical hepatocarcinogenesis. *Cell.* 2005;121(7):977–90.
 17. Haybaeck J, Zeller N, Wolf MJ, Weber A, Wagner U, Kurrer MO, et al. A lymphotoxin-driven pathway to hepatocellular carcinoma. *Cancer Cell.* 2009;16(4):295–308.
 18. Park EJ, Lee JH, Yu GY, He G, Ali SR, Holzer RG, et al. Dietary and genetic obesity promote liver inflammation and tumorigenesis by enhancing IL-6 and TNF expression. *Cell.* 2010;140(2):197–208.
 19. Kwon HJ, Won YS, Park O, Chang B, Duryee MJ, Thiele GE, et al. Aldehyde dehydrogenase 2 deficiency ameliorates alcoholic fatty liver but worsens liver inflammation and fibrosis in mice. *Hepatology.* 2014;60(1):146–57.
 20. Pikarsky E, Porat RM, Stein I, Abramovitch R, Amit S, Kasem S, et al. NF-kappaB functions as a tumour promoter in inflammation-associated cancer. *Nature.* 2004;431(7007):461–66.
 21. Knight B, Yeoh GC, Husk KL, Ly T, Abraham LJ, Yu C, et al. Impaired preneoplastic changes and liver tumor formation in tumor necrosis factor receptor type 1 knockout mice. *J Exp Med.* 2000;192(12):1809–18.
 22. Cheng K, Cai N, Zhu J, Yang X, Liang H, Zhang W. Tumor-associated macrophages in liver cancer: From mechanisms to therapy. *Cancer Commun (Lond).* 2022;42(11):1112–40.
 23. Fontanet P, Irala D, Alsina FC, Paratcha G, Ledda F. Pea3 transcription factor family members Etv4 and Etv5 mediate retrograde signaling and axonal growth of DRG sensory neurons in response to NGF. *J Neurosci.* 2013;33(40):15940–51.
 24. Lu YX, Ju HQ, Liu ZX, Chen DL, Wang Y, Zhao Q, et al. Correction: ME1 Regulates NADPH Homeostasis to Promote Gastric Cancer Growth and Metastasis. *Cancer Res.* 2019;79(14):3789.
 25. Sun Y, Wu L, Zhong Y, Zhou K, Hou Y, Wang Z, et al. Single-cell landscape of the ecosystem in early-relapse hepatocellular carcinoma. *Cell.* 2021;184(2):404–21 e16.
 26. Aran D, Hu Z, Butte AJ. xCell: digitally portraying the tissue cellular heterogeneity landscape. *Genome Biol.* 2017;18(1):220.
 27. Li XF, Chen C, Xiang DM, Qu L, Sun W, Lu XY, et al. Chronic inflammation-elicited liver progenitor cell conversion to liver cancer stem cell with clinical significance. *Hepatology.* 2017;66(6):1934–51.
 28. Liou GY, Doppler H, Necela B, Edenfield B, Zhang L, Dawson DW, et al. Mutant KRAS-induced expression of ICAM-1 in pancreatic acinar cells causes attraction of macrophages to expedite the formation of precancerous lesions. *Cancer Discov.* 2015;5(1):52–63.
 29. Yu LX, Ling Y, Wang HY. Role of nonresolving inflammation in hepatocellular carcinoma development and progression. *NPJ Precis Oncol.* 2018;2(1):6.
 30. Sun B, Karin M. Obesity, inflammation, and liver cancer. *J Hepatol.* 2012;56(3):704–13.
 31. Arthur JS, Ley SC. Mitogen-activated protein kinases in innate immunity. *Nat Rev Immunol.* 2013;13(9):679–92.
 32. Johnson GL, Lapadat R. Mitogen-activated protein kinase pathways mediated by ERK, JNK, and p38 protein kinases. *Science.* 2002;298(5600):1911–12.
 33. Lee JC, Laydon JT, McDonnell PC, Gallagher TF, Kumar S, Green D, et al. A protein kinase involved in the regulation of inflammatory cytokine biosynthesis. *Nature.* 1994;372(6508):739–46.
 34. Dumortier M, Ladam F, Damour I, Vacher S, Bieche I, Marchand N, et al. ETV4 transcription factor and MMP13 metalloprotease are interplaying actors of breast tumorigenesis. *Breast Cancer Res.* 2018;20(1):73.
 35. Cosi I, Pellicchia A, De Lorenzo E, Torre E, Sica M, Nesi G, et al. ETV4 promotes late development of prostatic intraepithelial neoplasia and cell proliferation through direct and p53-mediated downregulation of p21. *J Hematol Oncol.* 2020;13(1):112.

36. Xu X, Wang B, Liu Y, Jing T, Xu G, Zhang L, et al. ETV4 potentiates nuclear YAP retention and activities to enhance the progression of hepatocellular carcinoma. *Cancer Lett.* 2022;537:215640.
37. Kim E, Kim D, Lee JS, Yoe J, Park J, Kim CJ, et al. Capicua suppresses hepatocellular carcinoma progression by controlling the ETV4-MMP1 axis. *Hepatology.* 2018;67(6):2287–301.
38. Wang Y, Ding X, Liu B, Li M, Chang Y, Shen H, et al. ETV4 overexpression promotes progression of non-small cell lung cancer by upregulating PXN and MMP1 transcriptionally. *Mol Carcinog.* 2020;59(1):73–86.
39. Yang Y, Guo Y, Tan S, Ke B, Tao J, Liu H, et al. beta-Arrestin1 enhances hepatocellular carcinogenesis through inflammation-mediated Akt signalling. *Nat Commun.* 2015;6:7369.
40. Nakagawa H, Umemura A, Taniguchi K, Font-Burgada J, Dhar D, Ogata H, et al. ER stress cooperates with hypernutrition to trigger TNF-dependent spontaneous HCC development. *Cancer Cell.* 2014;26(3):331–43.
41. Xie M, Lin Z, Ji X, Luo X, Zhang Z, Sun M, et al. FGF19/FGFR4-mediated elevation of ETV4 facilitates hepatocellular carcinoma metastasis by upregulating PD-L1 and CCL2. *J Hepatol.* 2023.
42. Du L, Ji Y, Xin B, Zhang J, Lu LC, Glass CK, et al. Shp2 Deficiency in Kupffer Cells and Hepatocytes Aggravates Hepatocarcinogenesis by Recruiting Non-Kupffer Macrophages. *Cell Mol Gastroenterol Hepatol.* 2023;15(6):1351–69.
43. Nguyen-Lefebvre AT, Ajith A, Portik-Dobos V, Horuzsko DD, Arbab AS, Dzutsev A, et al. The innate immune receptor TREM-1 promotes liver injury and fibrosis. *J Clin Invest.* 2018;128(11):4870–83.
44. Yu J, Green MD, Li S, Sun Y, Journey SN, Choi JE, et al. Liver metastasis restrains immunotherapy efficacy via macrophage-mediated T cell elimination. *Nat Med.* 2021;27(1):152–64.
45. Williams M, Bonnardel J, Haest B, Vanderborght B, Wagner C, Remmerie A, et al. Spatial proteogenomics reveals distinct and evolutionarily conserved hepatic macrophage niches. *Cell.* 2022;185(2):379–96 e38.
46. Wen Y, Lambrecht J, Ju C, Tacke F. Hepatic macrophages in liver homeostasis and diseases-diversity, plasticity and therapeutic opportunities. *Cell Mol Immunol.* 2021;18(1):45–56.
47. Giese MA, Hind LE, Huttenlocher A. Neutrophil plasticity in the tumor microenvironment. *Blood.* 2019;133(20):2159–67.

SUPPORTING INFORMATION

Additional supporting information can be found online in the Supporting Information section at the end of this article.

How to cite this article: Qi D, Lu M, Xu P, Yao X, Chen Y, Gan L, et al. Transcription factor ETV4 promotes the development of hepatocellular carcinoma by driving hepatic TNF- α signaling. *Cancer Commun.* 2023;43:1354–1372. <https://doi.org/10.1002/cac2.12482>